

# Strain-Controlled Fatigue Behavior of ASTM A36 and A514 Grade F Steels and 5083-0 Aluminum Weld Materials

*For steel weld materials, tensile and strain-controlled fatigue properties vary with hardness and, although the hardness relationships for aluminum vary from steel, the mean stress relaxation behavior of all weld materials is found to be a function of the same material parameters*

BY Y. HIGASHIDA, J. D. BURK, AND F. V. LAWRENCE, JR.

**ABSTRACT.** The tensile and strain-controlled fatigue properties of base metal (BM), weld-metal (WM), and heat-affected zone (HAZ) material were determined for weldments of ASTM A36 and A514 grade F steels and 5083-0 aluminum. The mean stress relaxation behavior of these weld materials was also investigated. The HAZ properties were determined from specimens produced using a weld thermal-cycle simulator. The WM properties were obtained using specimens machined from weld metal deposits.

For the steel weld materials, the tensile and strain-controlled fatigue properties were found to vary with hardness. The fatigue resistance at lives greater than the transition fatigue life was found to increase as the hardness of the steel weld materials (BM's, WM's, HAZ's) increased. Properties of BM and WM for the 5083-0 aluminum welds did not obey the hardness relationships found for the steels, but the mean stress relaxation behavior of all the weld materials considered was found to be a function of the same material parameters.

## Introduction

The most common sites for fatigue crack initiation in welds are the weld toe, the weld root, or internal discontinuities.<sup>1-4</sup> In the first case, the crack initiates in untempered weld metal (WM) or grain coarsened heat-affected zone<sup>5</sup> (HAZ) near the edge of the weld reinforcement and then

propagates through the HAZ and base metal (BM). In the latter cases, the crack initiates and propagates in tempered weld metal. These sites are shown schematically in Fig. 1.

Previous studies of the fatigue behavior of weldments, summarized by Gurney<sup>2</sup> and Pollard and Cover,<sup>3</sup> have dealt with fatigue behavior of weldments without separating the effects of WM and HAZ microstructures. Only a limited number of studies have been undertaken to study the fatigue behavior of WM and HAZ, and most of these have been studies of fatigue crack propagation which have shown that the HAZ does not strongly influence the crack propagation rate.<sup>6-12</sup> Most studies of fatigue crack initiation in WM and HAZ using smooth specimens have been conducted under stress control<sup>13-18</sup>.

Weld toe fatigue cracks usually initiate in the grain coarsened region of the heat affected zone (hereafter HAZ).<sup>19</sup> The width of the grain coarsened region in the welded joint is too small to permit direct measurements of strain-controlled fatigue properties. For A514 welds, the width of the coarsened region is about 0.05 in. (1.3 mm)

or less. It was necessary, therefore, to reproduce the weld thermal cycle in a smooth specimen large enough for the normal methods of strain controlled fatigue testing.

Three methods have been commonly employed to reproduce HAZ microstructures in test specimens: furnace heating,<sup>6-9,11</sup> high frequency induction heating,<sup>17,18,20</sup> and direct resistance heating.<sup>21-25</sup> The direct resistance heating method was judged most suitable and was used in this investigation.

## Strain Controlled Fatigue Properties

The smooth specimen fatigue behavior of a metal tested under reversed strain control may be characterized by four material parameters,<sup>26-28</sup> which relate the strain amplitude ( $\epsilon_a$ ) to the failure life ( $2N_f$ )—see Table 1:

$$\epsilon_a = \epsilon'_f (2N_f)^c + \frac{\sigma'_f}{E} (2N_f)^b \quad (1)$$

Mean stress ( $\sigma_a$ ) effects may be included through the modification<sup>29</sup>:

$$\epsilon_a = \epsilon'_f (2N_f)^c + \frac{(\sigma'_f - \sigma_a)}{E} (2N_f)^b \quad (2)$$

where  $\epsilon'_f$  and  $c$  are the fatigue ductility coefficient and exponent, and  $\sigma'_f$  and  $b$  are the fatigue strength coefficient and exponent. An additional useful index of fatigue resistance is the transition fatigue life ( $2N_{f,t}$ ) which is the life of a smooth specimen under strain control at which the elastic ( $\Delta \epsilon_e/2$ ) and plastic ( $\Delta \epsilon_p/2$ ) strain amplitudes are identical.

Y. HIGASHIDA is Research Engineer, Hiratsuka Research Laboratory, Sumitomo Heavy Industries, Ltd., Japan; J. D. BURK is Lead Engineer, Materials and Processes Department, McDonnell Douglas Astronautics Co., St. Louis, Missouri; F. V. LAWRENCE, JR. is Professor, Department of Metallurgy and Mining and Civil Engineering, at the University of Illinois, Urbana-Champaign, Illinois.

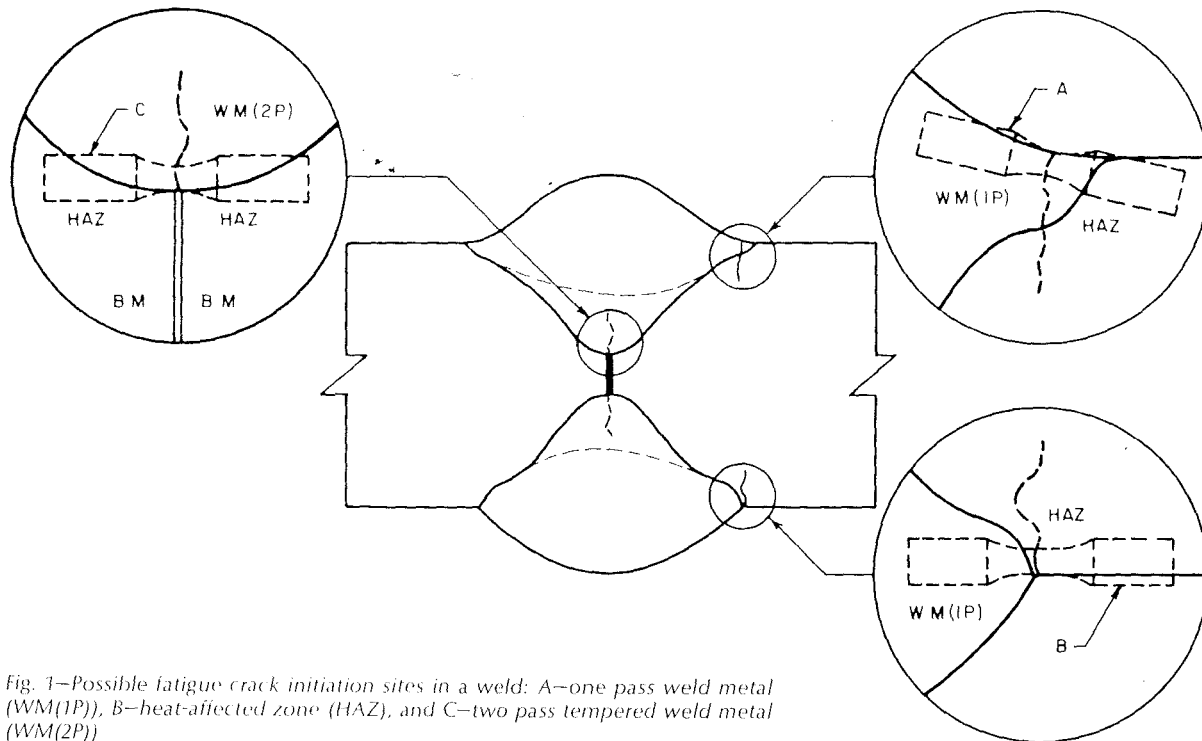


Fig. 1—Possible fatigue crack initiation sites in a weld: A—one pass weld metal (WM(1P)), B—heat-affected zone (HAZ), and C—two pass tempered weld metal (WM(2P))

$$2N_{ir} = \left( \frac{\epsilon'_r E}{\sigma'_r} \right)^{\frac{1}{b-c}} \quad (3)$$

As shown by equation (2), the mean stress ( $\sigma_m$ ) has an influence on crack initiation life. The mean stress ( $\sigma_m$ ) at any reversal ( $2N$ ) has been shown to relax according to the power function:<sup>26,30</sup>

$$\sigma_{m, 2N} = \sigma_{m, i} (2N-1)^k \quad (4)$$

where  $\sigma_{m, i}$  is the initial mean stress and  $k$  is the relaxation exponent which is dependent on strain amplitude ( $\epsilon_a$ ).

The monotonic and cyclic stress-strain properties of a material may be represented by elastic and plastic strain components as:<sup>28</sup>

Monotonic

$$\epsilon = \frac{\sigma}{E} + \left( \frac{\sigma}{K} \right)^{\frac{1}{n}} \quad (5)$$

Cyclic

$$\epsilon_a = \frac{\sigma_a}{E} + \left( \frac{\sigma_a}{K'} \right)^{\frac{1}{n'}} \quad (6)$$

where  $K$  ( $K'$ ) and  $n$  ( $n'$ ) are the monotonic (cyclic) strength coefficient and strain-hardening exponent.

#### Object and Scope

ASTM A36 and A514 steels and 5083-0 aluminum were chosen for study because:

1. A36 steel is a typical construction grade ferritic-pearlitic steel widely used for land vehicles and structures and is easily welded without

special heat treatments.

2. A514 steel is a typical, constructional grade, low-alloy, martensitic steel widely used for pressure vessels and structures and is also readily welded.

3. 5083-0 aluminum is a readily weldable hardening aluminum alloy used in cryogenic applications.

Completely reversed, uniaxial strain-controlled tests of the smooth specimens were employed to study fatigue behavior of BM, HAZ, and one- and two-pass WM's for A36 and A514 welds and BM and WM behavior of 5083-0 welds. Mean stress relaxation tests were also conducted for each material at a constant mean strain and at various strain amplitudes.

### Experimental Program

#### Specimen Preparation

Base metal specimens of A514 steel (A514-BM) and 5083-0 aluminum (5083-0-BM) were machined from  $\frac{3}{4}$  in. (19 mm) and 1 in. (25 mm) thick plate keeping their axes parallel to the rolling direction of the plate—Fig. 2A. The HAZ specimens were machined from base plate and then subjected to the simulated weld thermal cycles after which they were machined to the final dimensions as shown in Fig. 2B. Heat-affected zone specimens of 5083 aluminum base metal were not made.

Five series of weld metal specimens were prepared: E60S-3-WM(1P) was machined from a one-pass butt welded joint of A36 steel plates using a  $\frac{1}{16}$  in. (1.6 mm) diameter E60S-3 elec-

trode; E60S-3-WM(2P) was machined from a two-pass butt welded joint of A36 steel plates using the same electrode as E60S-3-WM(1P); E110-WM(1P) was machined from a one-pass butt weld of A514 steel using a  $\frac{1}{16}$  in. (1.6 mm) diameter E110 electrode; E110-WM(2P) was machined from a two-pass butt weld of A514 steel using the E110 electrode; and 5183-WM was machined from a two-pass double-V butt weld of 5083-0 aluminum using a 5183 electrode.

All welding was in the flat position using gas metal arc (GMA) processes. After welding, the weld deposits were radiographed to check for internal defects. The welded plates were then saw-cut into blanks with their axes normal to the welding axis. The blanks were then machined to the dimensions shown in Fig. 2A for monotonic tension tests and Fig. 2C for fatigue tests.

Chemical compositions are shown in Table 2, and the welding parameters are listed in Table 3.

#### Simulation of HAZ

The weld thermal cycle at the HAZ adjacent to the fusion line was measured. Chromel-alumel thermocouples (0.020 in. (0.51 mm) diameter) were spot welded onto the surface of a A36 or A514 steel plate near the fusion line. The location of the thermocouple was determined by preliminary measurements to define the fusion line position. The thermocouples were electrically and thermally shielded and were connected to an oscilloscope. The thermal cycle was photographical-

**Table 1—List of symbols**

$\sigma, \epsilon$	True stress and strain
$\epsilon_a, \epsilon_{tr}, \epsilon_m$	Strain amplitude, transition strain, and mean strain
$\Delta \epsilon_p / 2$	Plastic strain amplitude
$\sigma_0$	Mean stress
$\sigma_{0.1}, \sigma_{0.2N}$	Initial and current mean stress
$2N_f, 2N_{tr}, 2N$	Reversals to failure, transition fatigue life, reversals
$K, K'$	Monotonic and cyclic strength coefficient
$n, n'$	Monotonic and cyclic strain hardening exponent
$E$	Elastic modulus
$\epsilon_f, \sigma_f$	True strain and stress at fracture
$\epsilon'_f, \sigma'_f$	Fatigue ductility and strength coefficients
$c, b$	Fatigue ductility and strength exponent
$k$	Relaxation exponent
BHN, DPH	Brinnell and diamond pyramid hardness number
$S_u, \sigma_y'$	Ultimate strength and cyclic yield stress

ly recorded. Typical traces are shown in Fig. 3.

A weld thermal cycle simulator was developed (Fig. 4) to reproduce uniformly the measured weld thermal cycle in a specimen large enough for monotonic tension and fatigue tests. The specimen in (Fig. 2A) was held in a pair of water-cooled OFHC copper grips. The grips and specimen were mounted on a wooden stand and fixed to prevent transverse distortion of the specimen at high temperatures but not longitudinal movement. The specimen was heated by a current from the secondary of the step down transformer (Fig. 4), and the temperature was measured by a thermocouple spot welded to the center of the specimen. The heating rate was controlled by setting the temperature controller to some fraction of total output.

When the temperature of the specimen reached the maximum temperature desired, the current was shut off; and the specimen was allowed to cool. The cooling rate was controlled by the flow of the grip cooling water and the

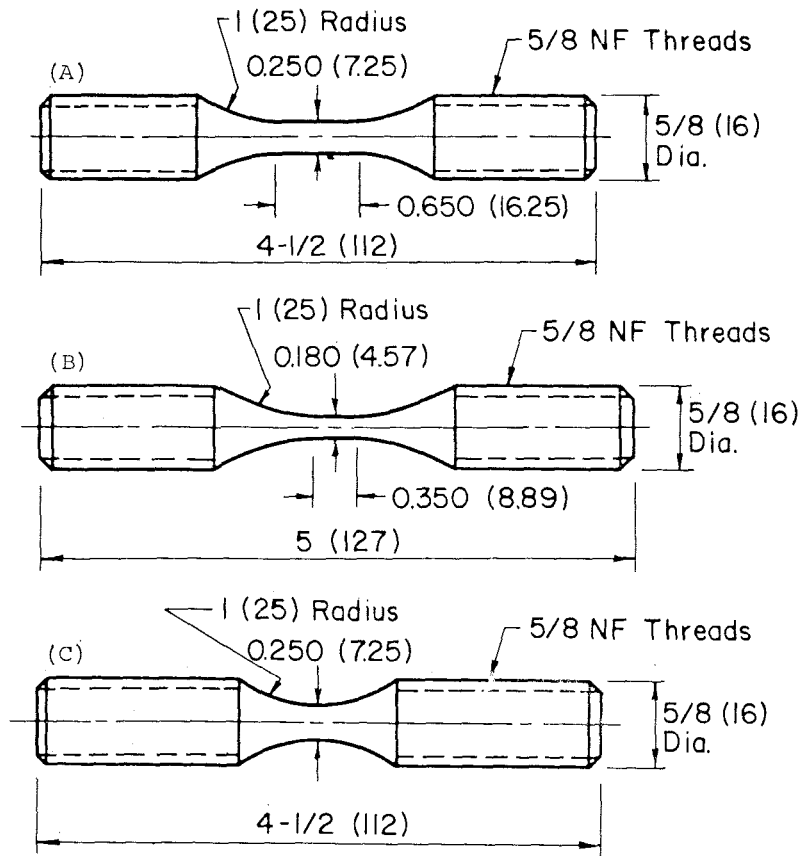


Fig. 2—Smooth specimens of A—base metal, B—heat-affected zone, and C—weld metal materials; all dimensions are in inches (mm)

**Table 2—Chemical Compositions of Base and Filler Metals, Wt-%**

Material	C	Mn	P	S	Si	Ni	Cr	Mo	Cu	Fe
ASTM A36 <sup>(a)</sup>	0.21	1.1	0.12	0.021	<0.10	<0.10	<0.08	<0.10	0.10	Bal.
E60S-3	0.09	1.0	0.017	0.024	0.50	—	—	—	—	Bal.
ASTM A514 <sup>(a)</sup>	0.20	0.82	0.010	0.016	0.24	0.08	0.51	0.20	<0.01	Bal.
E110	0.08	1.70	0.005	0.009	0.46	2.40	0.05	0.50	—	Bal.
	Si	Fe	Cu	Mn	Mg	Cr	Zn	Ti	Zr	Al
ASTM 5083-0	0.14	0.22	0.05	0.64	4.50	0.08	0.04	0.03	<0.001	Bal.
5183	0.12	0.17	0.02	0.57	4.96	0.07	0.03	0.09	—	Bal.

<sup>(a)</sup>Compositions based on chemical analysis—others are typical as supplied compositions.

flow of argon gas directed onto the specimen. Once the correct condition was determined, it was possible to subject specimens to reproducible weld thermal cycles such as that shown in Fig. 3.

Hardness and metallographic studies were performed on the simulated

HAZ specimens and compared with the actual weld HAZ. Figure 5 shows the results of a Vickers Pyramid hardness traverse 0.1 mm (0.004 in.) below the plate surface for A36 and A514 one-pass butt welds. The results of a hardness traverse for A36 and A514 simulated HAZ specimens are shown

**Table 3—Welding Parameters**

Weld (base/filler metal)	Plate thickness, mm <sup>(a)</sup>	Electrode diameter, mm <sup>(a)</sup>	Voltage, V	Current, A	Travel speed, mm/miq. <sup>(a)</sup>	Preheat temperature, (°C)	Heat input, kJ/mm <sup>(a)</sup>	Shielding gas composition, vol-%
A36/E60S-3	22.2	1.59	35	500	370	22	2.80	Ar-2% O <sub>2</sub>
A514F/E110	19.1	1.59	30	290	432	96	1.20	Ar-2% O <sub>2</sub>
5083-0/5183	25.4	1.59	24	280	420	22	0.95	He-25% Ar

<sup>(a)</sup>1 mm = 0.04 in.

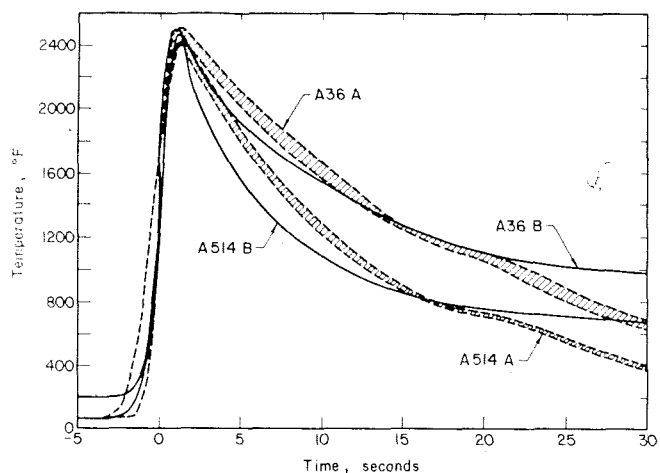


Fig. 3—Simulated (A) and measured (B) weld thermal cycles for A514 grade F and A36 steel welds

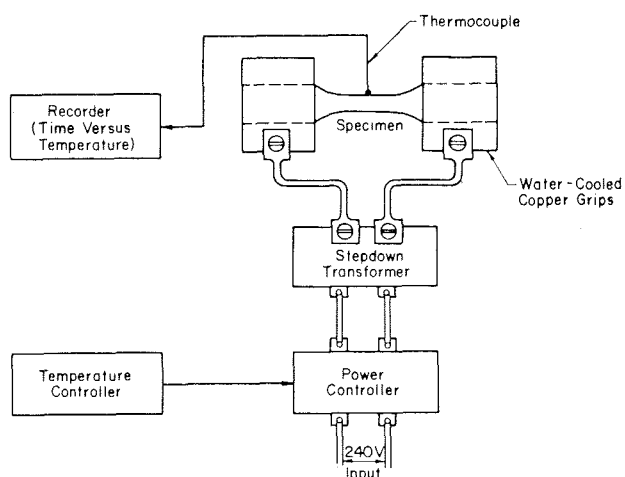


Fig. 4—Schematic of weld thermal cycle simulator

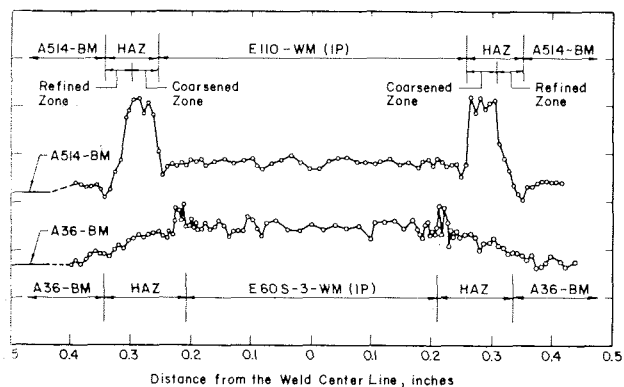


Fig. 5—Vickers hardness survey 0.1 mm below the weld plate surface for A514 and A36 butt welds

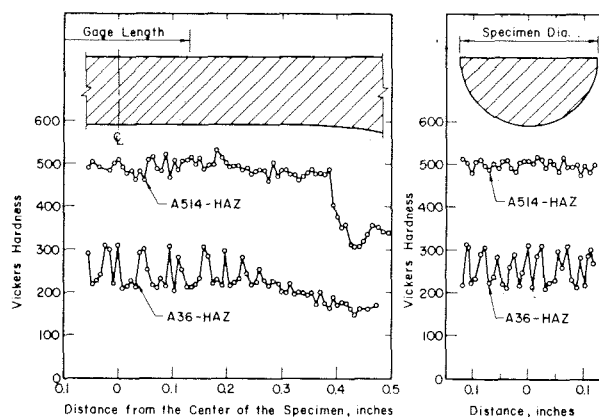


Fig. 6—Vickers hardness survey along the axis and across the diameter of both A514 and A36 simulated HAZ smooth specimens

Fig. 6 which indicates that the simulated HAZ specimens were homogeneous in hardness within the gage length.

Both average values and ranges in hardness numbers inside the gage length of each specimen were very close to those of each actual weld HAZ (Figs. 5 and 6). For example, the average hardness numbers of the actual HAZ (grain-coarsened region) and simulated HAZ within the gage length were 257 DPH and 255 DPH for the A36 steel, respectively, and 497 DPH and 496 DPH for the A514 steel. Hardness values for the A514, A36, and 5083-0 weld materials are listed in

Tables 4 to 6.

Metallographic examination was carried out on both the actual weld HAZ and the simulated HAZ specimens. Excellent correlation was observed in comparison between the actual weld HAZ and the simulated HAZ microstructures.

#### Mechanical Testing

Tension tests were conducted using a 20 kip MTS hydraulic test system similar to that described by Feltner and Mitchell.<sup>31</sup> A clip-on extensometer (0.5

in. (12.7 mm) gage length) was used to measure strain for the base and weld metal cylindrical specimens, while a 0.26 in. (6.6 mm) gage length extensometer was used for the HAZ specimens. The weld metal specimens were hourglass-shaped and required the measurement of diametric strain and its conversion to axial strain by means of an analog computer.<sup>32</sup>

Fatigue tests were conducted with the same apparatus used for monotonic tension tests. Axial strain was controlled for the smooth specimens of A514, A36, and 5083-0 weld materi-

Table 4—Tensile Properties of Base, Weld, and Heat-Affected Materials for ASTM A514F/E110 Welds

Material	A514-BM	A514-HAZ	E110-WM(1P)	E110-WM(2P)
Hardness, DPH/BHN	320/303	496/461	382/362	327/310
Modulus of elasticity, $E$ , $\times 10^4$ ksi (MPa)	30.3 (210)	30.3 (210)	30.3 (210)	30.3 (210)
0.2% offset yield strength, ksi (MPa)	129 (890)	171 (1180)	121 (835)	110 (760)
Ultimate tensile strength, $S_u$ , ksi (MPa)	136 (938)	204 (1408)	150 (1035)	132 (910)
Reduction in area, %	63.0	52.7	57.6	59.3
True fracture strength, $\sigma_f$ , ksi (MPa)	216 (1490)	326 (2250)	320 (2208)	241 (1663)
True fracture ductility, $\epsilon_f$	0.994	0.750	0.857	0.899
Strain hardening exponent, $n$	0.060	0.092	0.092	0.085
Strength coefficient, $K$ , ksi (MPa)	172 (1187)	306 (2110)	226 (1560)	187 (1290)

**Table 5—Tensile Properties of Base, Weld, and Heat-Affected Materials for ASTM A36/E605-3 Butt Welds**

Material	A36-BM	A36-HAZ	E605-3-WM(1P)	E605-3-WM(2P)
Hardness, DPH/BHN	168/160	255/243	245/233	211/201
Modulus of elasticity, $E$ , $\times 10^3$ ksi (MPa)	27.5 (190)	27.4 (189)	27.4 (189)	27.4 (189)
0.2% offset yield strength, ksi (MPa)	32.5 (224)	77.5 (534)	84.1 (580)	59.2 (408)
Ultimate tensile strength, $S_u$ , ksi (MPa)	60.0 (414)	96.7 (667)	103 (710)	84.0 (580)
Reduction in area, %	69.7 (481)	52.5 (362)	44.6 (308)	60.7 (419)
True fracture strength, $\sigma_f$ , ksi (MPa)	138 (952)	133 (918)	143 (987)	147 (1014)
True fracture ductility, $\epsilon_f$	1.19	0.745	0.590	0.933
Strain hardening exponent, $n$	0.0146/0.258	0.102	0.098	0.130
Strength coefficient, $K$ , ksi (MPa)	113 (780)	142 (980)	143 (987)	123 (849)

**Table 6—Tensile Properties of Base and Weld Metal Materials for ASTM 5083-0/5183 Aluminum Welds**

Property	5083-BM	5183-WM
Hardness, DPH/BHN	106/93	105/92
Modulus of Elasticity, $E \times 10^3$ ksi (MPa)	10.3 (71)	10.3 (71)
0.2% offset yield strength, ksi (MPa)	19 (131)	20 (138)
Ultimate tensile strength, $S_u$ , ksi (MPa)	42.6 (294)	43.3 (299)
Reduction in area, %	30	33
True fracture strength, $\sigma_f$ , ksi (MPa)	60 (414)	61 (421)
True fracture ductility, $\epsilon_f$	0.36	0.40
Strain hardening exponent, $n$	0.129	0.133
Strength coefficient, $K$ , ksi (MPa)	43.4 (300)	44.5 (307)

als as previously discussed. A sine-wave function generator was used to generate the strain or stress history. Test frequencies varied from 0.1 to 10 Hz. Stress-strain hysteresis loops were recorded at intervals to determine cycle-dependent changes in stress and plastic strain amplitudes.

Mean stress relaxation tests with constant mean strain but variable strain amplitude were conducted. A typical strain-block-sequence used is shown in Fig. 7. A stabilization block was applied to each specimen to ensure stabilization of the hysteresis loop before inducing a mean stress

and studying its relaxation behavior. Each initial mean stress of the mean stress relaxation blocks was induced by applying a mean strain. Mean stress ( $\sigma_m$ ) as a function of cycles was then measured under a constant strain amplitude.

## Results

### Monotonic Stress-Strain Behavior

Tensile properties of A36, A514, and 5083-0 weld materials are listed in Tables 4 to 6. The monotonic true stress-strain curves for the ten micro-

structures studied are shown in Figs. 8 to 10. For the A36 weld materials (Fig. 8), the E605-3-WM(1P) has the highest yield and ultimate strength, the A36-HAZ has the second, and the A36-BM has the lowest.

The order for higher true fracture ductility is opposite. For the A514 weld materials (Fig. 9), the order for higher ultimate tensile strength and lower true fracture ductility is: A514-HAZ, E110-WM(1P), A514-BM, and E110-WM(2P). However, the order for higher yield strength is: A514-HAZ, A514-BM, E110-WM(1P), and E110-WM(2P).

For the 5083-0 weld materials (Fig. 10), the strength, ductility, and ultimate strength are essentially identical for base and weld metal.

In general, the strength and ductility of the weld materials are relatable to the hardness—Tables 4 to 6.

### Cyclic Stress-Strain Behavior

The cyclic stress-strain curves obtained for each material are shown with each of the respective tensile stress-strain curves in Figs. 8 to 10. All A36 and A514 weld materials (except A36-BM and A36-WM(2P)) show varying degrees of cyclic softening, while the 5083-0 weld materials show a large amount of cyclic hardening. The cyclic yield strength ( $\sigma'_y$ ) was obtained by curve fitting  $\sigma'_y$  as a function of the Brinell hardness number (BHN):

$$\sigma'_y = -18.4 + 0.331 \text{ BHN (ksi)} \quad (7)$$

Equation 7 is valid for the A36 and A514 materials but does not apply to the 5083-0 materials.

### Fatigue Behavior

The fatigue properties for the A36, A514, and 5083-0 weld materials are given in Tables 7 to 9. The fatigue strength coefficient ( $\sigma'_f$ ) and the fatigue strength exponent ( $b$ ) were calculated as a function of reversals to failure using a least-squares fit to the measured elastic strain data. The fatigue ductility coefficients ( $\epsilon'_f$ ) and the fatigue ductility exponent ( $c$ ) were obtained in a similar manner using the plastic strain data and the number of reversals to failure. Excellent agree-

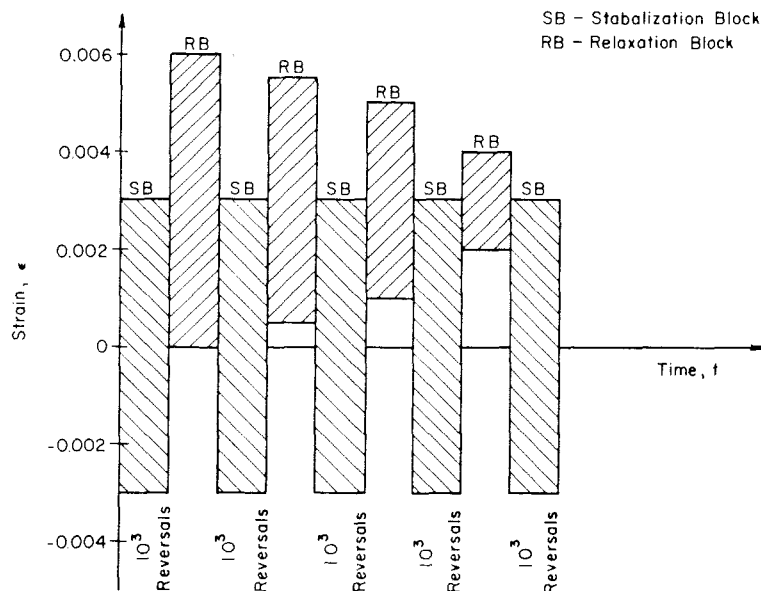


Fig. 7—Strain control history for mean stress relaxation test of aluminum 5183-WM

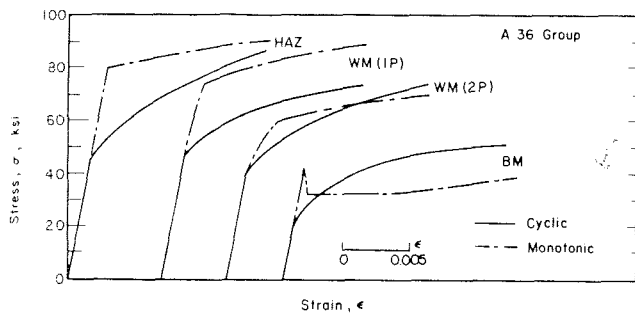


Fig. 8—Monotonic and cyclic stress-strain response for A36 steel weld materials

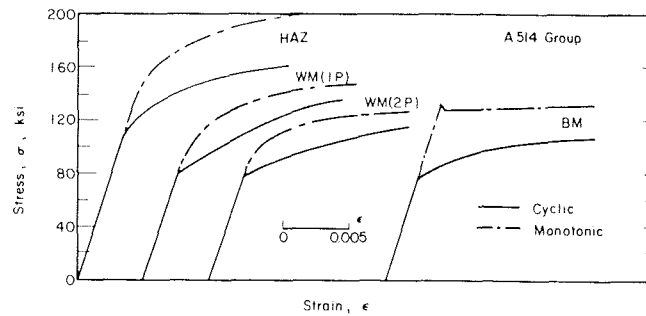


Fig. 9—Monotonic and cyclic stress-strain response for A514 steel weld materials

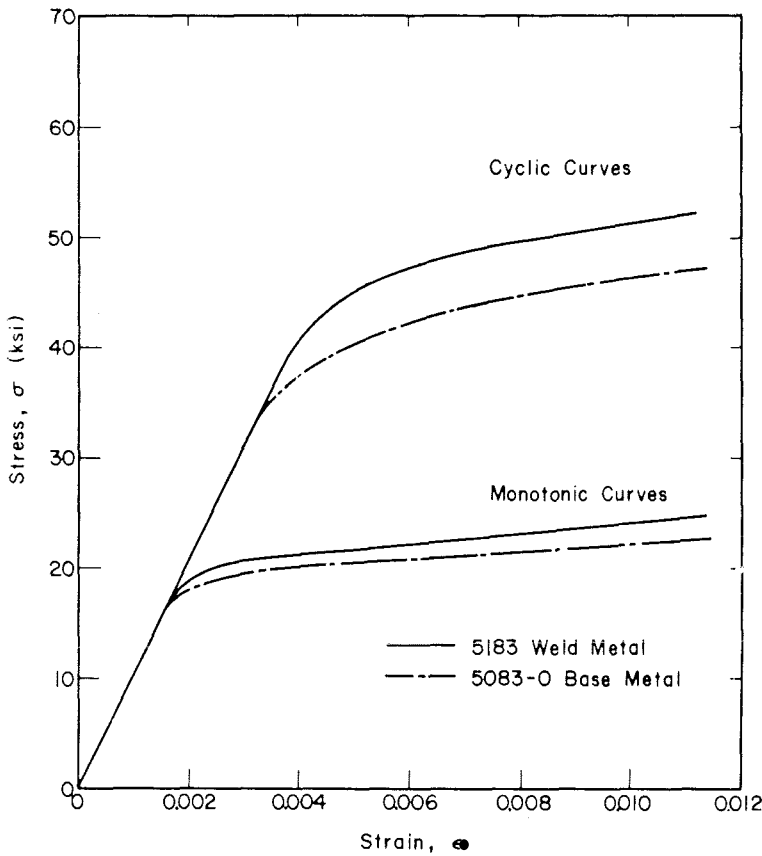


Fig. 10—Monotonic and cyclic stress-strain response for 5083-0 aluminum weld materials

ment was obtained between the experimental data and equation (1) as seen in Figs. 11 to 13.

For the A36 weld materials (Fig. 11), A36-WM(1P) has the highest fatigue resistance for all lives. The curve of A36-WM(2P) is similar to that of A36-

WM(1P), but always lies below the former. For A36-BM and A36-HAZ, the higher hardness materials have the higher fatigue resistance at long lives but a lower fatigue resistance at short lives. The A36-BM is inferior to the other materials in the A36 group, and

the difference in fatigue resistance between A36-BM and the others becomes largest at long lives.

For the A514 weld materials (Fig. 12), the relationship between hardness and fatigue resistance mentioned for A36-BM and A36-HAZ is also valid for A514-BM and A514-HAZ.

As seen in Fig. 12, A514-BM is slightly superior at short lives, A514-WM(2P) is slightly superior at intermediate lives, and A514-HAZ is significantly superior at long lives. A514-WM(1P) is always inferior at the lives greater than about 200 reversals.

For the A514 weld materials (Fig. 12), 13), the 5183-WM is very similar in fatigue behavior to the 5083-0 base metal with the base metal producing slightly greater fatigue resistance at the shorter lives. This result is not surprising considering the similar hardness (Table 6) of the two materials.

#### Mean Stress Relaxation Behavior Test Results

The results of a typical mean stress test, conducted at a positive mean strain, are shown in Fig. 14. The lines were obtained by least-squares fit of the data to conform to the power function of equation (4). The relaxation exponent ( $k$ ) was calculated by a least-squares fit for mean stress relaxation test data for the A36, A514, and 5083-0 weld materials and are listed in Table 10.

As mentioned in previous studies,<sup>19,22</sup> it was observed that the strain amplitude influenced the cyclic mean stress relaxation behavior significantly, while mean strain did not. The relaxa-

Table 7—Cyclic and Fatigue Properties of Base, Weld, and Heat-Affected Materials for ASTM A514F/E110 Welds

Material	A514-BM	A514-HAZ	E110-WM(1P)	E110-WM(2P)
Cyclic yield strength, 0.2% offset, ksi (MPa)	87.6 (604)	136 (938)	94.2 (650)	87.4 (603)
Cyclic strain hardening exponent, $n'$	0.091	0.103	0.177	0.166
Cyclic strength coefficient, $K'$ , ksi (MPa)	158 (1090)	256 (1765)	293 (2021)	242 (1670)
Fatigue strength coefficient, $\sigma'_f$ , ksi (MPa)	189 (1305)	290 (2000)	274 (1890)	204 (1408)
Fatigue ductility coefficient, $\epsilon'_f$	0.975	0.783	0.848	0.595
Fatigue strength exponent, $b$	-0.079	-0.087	-0.115	-0.079
Fatigue ductility exponent, $c$	-0.699	-0.713	-0.734	-0.590
Transition fatigue life, $2N_{1r}$ , reversals	3,461	1,138	1,536	6,448

**Table 8—Cyclic and Fatigue Properties of Base, Weld, and Heat-Affected Materials for ASTM A36/E60S-3 Welds**

Material	A36-BM	A36-HAZ	E60S-3-WM(1P)	E60S-3-WM(2P)
Cyclic yield strength, 0.2% offset, ksi (MPa)	33.6 (232)	58.2 (402)	55.8 (385)	52.6 (363)
Cyclic strain hardening exponent, $n'$	0.249	0.215	0.155	0.197
Cyclic strength coefficient, $K'$ , ksi (MPa)	159 (1097)	216 (1490)	146 (1007)	179 (1235)
Fatigue strength coefficient, $\sigma'_f$ , ksi (MPa)	147 (1014)	105 (724)	131 (904)	149 (1028)
Fatigue ductility coefficient, $\epsilon'_f$	0.271	0.218	0.607	0.602
Fatigue strength exponent, $b$	-0.132	-0.066	-0.075	-0.090
Fatigue ductility exponent, $c$	-0.451	-0.492	-0.548	-0.567
Transition fatigue life, $2N_{tr}$ , reversals	200,000	13,234	28,022	19,259

tion exponent ( $k$ ) is plotted in Fig. 15 as a function of the strain amplitude ( $\epsilon_a$ ) for all the materials studied.

From Fig. 15, it can be seen that the A36 weld materials have the greatest relaxation rate while the A514 weld materials have the least for a given strain amplitude. The relaxation behavior of the 5183-WM is intermediate. Materials with the higher transition fatigue lives, A36 weld materials (Tables 7 to 9), have the greater relaxation rates, while the materials with the shorter transition fatigue lives, A514 and 5183 weld materials, have the lower relaxation rates at a given strain amplitude.

**Discussion**

**Variation of Weld Materials Properties with Hardness**

The relationships between hardness and mechanical and fatigue properties—equation (2)—have been established by Landgraf<sup>33</sup> and Morrow *et al.*<sup>34</sup> for steels. A comparison of these known relationships between hardness and fatigue properties and the test results for A36 and A514 BM's, WM's, and HAZ's was made.

**Table 9—Cyclic and Fatigue Properties of Base and Weld Materials for ASTM 5083-0/5183 Aluminum Welds**

Material	5083-BM	5183-WM
Cyclic yield strength, 0.2% offset, ksi (MPa)	42 (290)	39 (269)
Cyclic strain hardening exponent, $n'$	0.114	0.072
Cyclic strength coefficient, $K'$ , ksi (MPa)	84 (580)	73.5 (507)
Fatigue strength coefficient, $\sigma'_f$ , ksi (MPa)	103 (711)	92.5 (638)
Fatigue ductility coefficient, $\epsilon'_f$	0.405	0.581
Fatigue strength exponent, $b$	-0.122	-0.107
Fatigue ductility exponent, $c$	-0.692	-0.890
Transition fatigue life, $2N_{tr}$ , reversals	640	205

Landgraf<sup>33</sup> found a linear relationship between the transition fatigue life ( $2N_{tr}$ ) and hardness which is shown by the solid line in Fig. 16. Both A36 and A514 weld materials conform to the linear relationship which is shown as a dashed extension of the solid line. The true fracture strength ( $\sigma_t$ ) has been found to be equal to half the Brinell hardness number (BHN) for steels<sup>33</sup> for low and intermediate hardnesses as shown in Fig. 17. The  $\sigma_t$  for the A36 and A514 weld materials was also found to obey this relationship (Fig. 17).

Values of the true fracture ductility

( $\epsilon_t$ ) were found to decrease with increases in hardness (Fig. 18). A single relationship, however, was not found for either the A36 and A514 weld materials or the steels previously investigated by Landgraf<sup>33</sup> (shown as dashed lines in Fig. 18). The monotonic strain hardening exponent ( $n$ ), also shown in Fig. 18, was found to be a parabolic function of hardness with its minimum occurring at 400 BHN.

The cyclic strain hardening exponent ( $n'$ ) was plotted vs. hardness (Fig. 19), and was found to decrease as the hardness increased for the A36 and A514 weld materials. No trend was

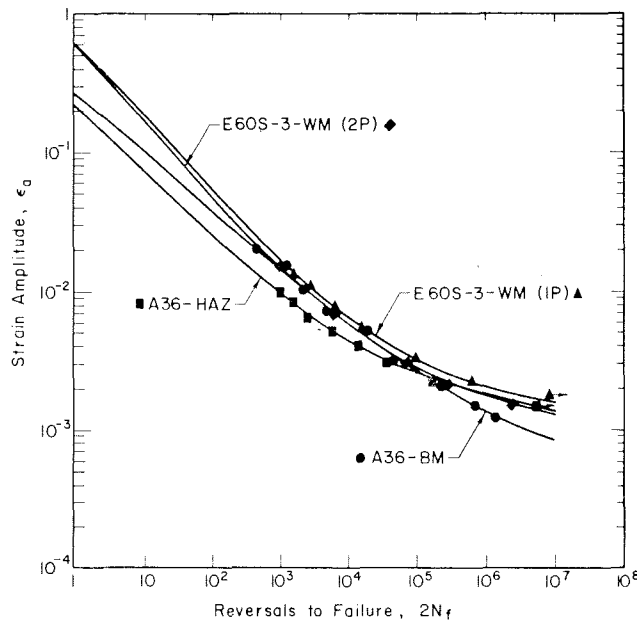


Fig. 11—Strain-life fatigue behavior of A36 steel weld materials

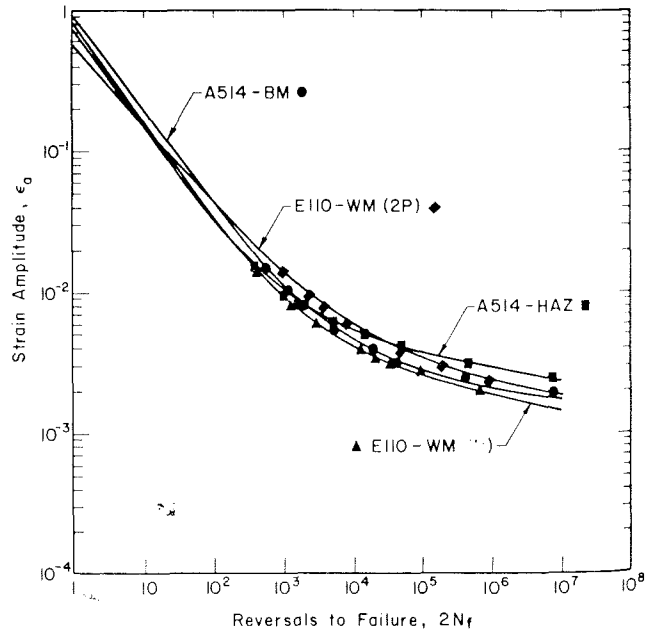


Fig. 12—Strain-life fatigue behavior of A514 steel weld materials

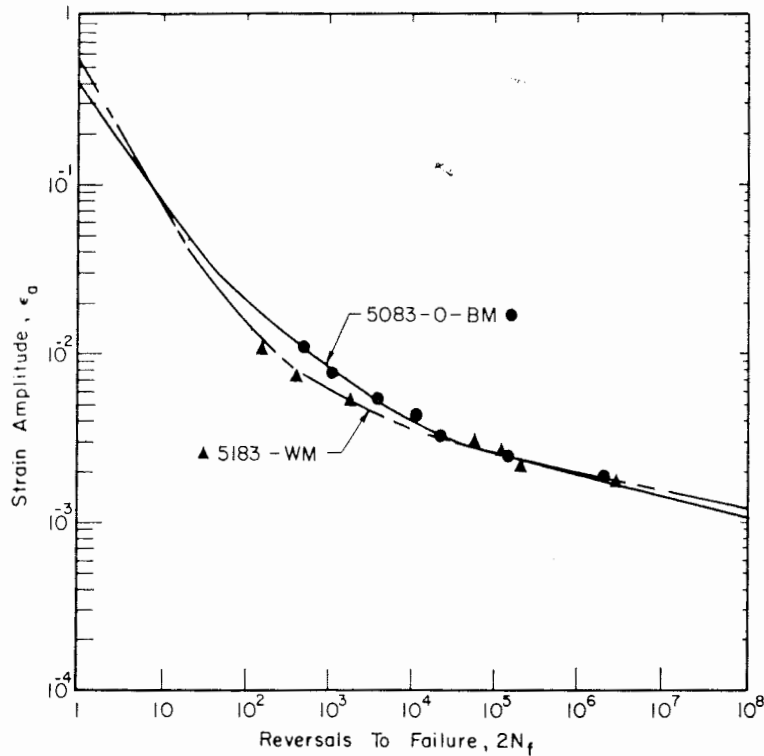


Fig. 13—Strain-life fatigue behavior of 5083-0 aluminum weld materials

reported by Landgraf, however, for higher hardness steels as shown by the steel scatter band in Fig. 19.

Based on hardness, the monotonic and cyclic properties ( $n$ ,  $\sigma_f$ ,  $\epsilon_f$ , and  $n'$ ) may be estimated. The fatigue strength ( $\sigma'_f$ ) and ductility ( $\epsilon'_f$ ) coefficients may be approximated by their monotonic counterparts.<sup>11</sup>

$$\sigma'_f \cong \sigma_f \quad (8)$$

$$\epsilon'_f \cong \epsilon_f \quad (9)$$

The cyclic strength coefficient is:<sup>28</sup>

$$K' = \frac{\sigma'_f}{(\epsilon'_f)n'} \quad (10)$$

The fatigue ductility ( $c$ ) and strength ( $b$ ) exponents are also functions of hardness for the A36 and A514 weld materials. The fatigue strength exponent increases as hardness increases as shown in Fig. 20, while the fatigue ductility exponent decreases as hard-

ness increases. These trends are consistent with the relationship:<sup>28</sup>

$$n' = \frac{b}{c} \quad (11)$$

and the observed decrease in  $n'$  with increasing hardness shown in Fig. 19.

#### Factors Influencing Mean Stress Relaxation Behavior

The mean stress relaxation behavior of a material has been found to be a function of the strain amplitude ( $\epsilon_a$ ).<sup>26,27,30</sup> Measured mean stress relaxation exponents—equation (4)—which determine the relaxation rate and mean stress fatigue damage behavior were plotted as a function of hardness in Fig. 21. Here it can be seen that  $k$  depends on hardness for the A514 weld materials but not for the A36 weld materials. However, by dividing the plastic strain amplitude (determined from the total strain amplitude) by the elastic modulus ( $E$ ) and transition strain ( $\epsilon_{tr}$ ) of the material, a linear relationship shown in Fig. 22 was obtained which appears to be valid for all the materials studied:<sup>27</sup>

$$K = 4625 (\text{ksi})^{-1} \frac{\Delta \epsilon_p / 2}{E \epsilon_{tr}}$$

The transition strain ( $\epsilon_{tr}$ ) is half the strain amplitude ( $\epsilon_a$ ) which corresponds to  $2N_{tr}$ .

#### Acknowledgments

This study has been supported in part by the University of Illinois Fracture Control Program; the U. S. Army Corps of Engineers, Grant DACA 88-75-C-0014; and the U. S. Navy-Naval

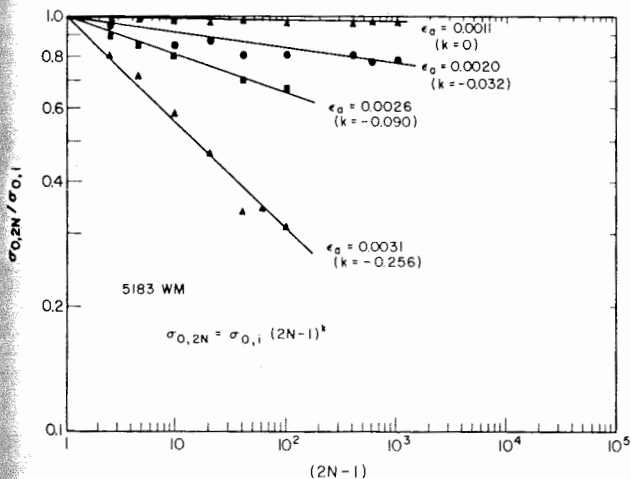


Fig. 14—Normalized mean stress relaxation test results for 5183 aluminum weld metal

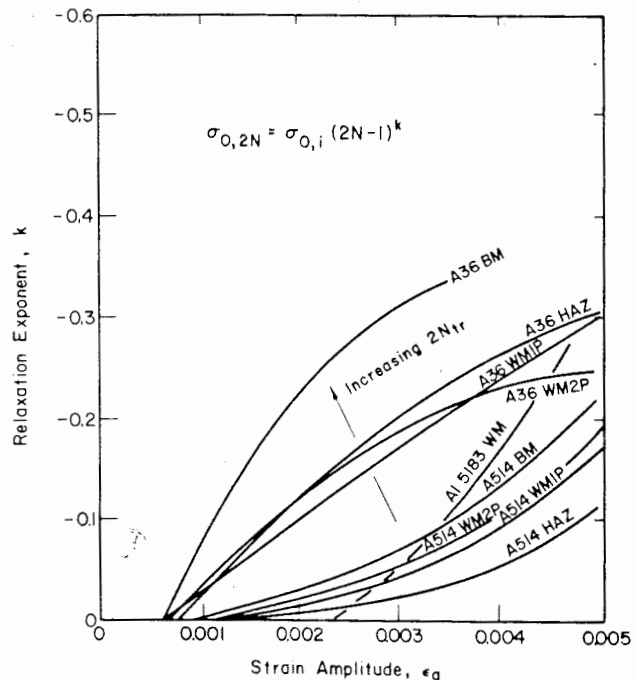


Fig. 15 (right)—Relaxation exponent ( $k$ ) as a function of the strain amplitude for A36, A514, and 5083-0 weld materials



Table 10—Cyclic Mean Stress Relaxation Exponent (k) for A514, A36, and 5083-0 Base and Weld Materials<sup>(a)</sup>

$\epsilon_a$	A514				A36				5083-0	
	BM	HAZ	WM(IP)	WM(2P)	BM	HAZ	WM(1P)	WM(2P)	BM	WM <sup>(b)</sup>
0.0010	0.009 (0.015)	0.007 (0.008)	0.009 (0.016)	0.012 (0.011)	0.012 (0.001)	0.030 (0.030)	0.030 (0.031)	0.028 (0.032)		0
0.0015	0.015 (0.025)	0.007 (0.008)	0.018 (0.017)	0.016 (0.011)	0.068 (0.046)	0.061 (0.060)	0.065 (0.065)	0.075 (0.063)		
0.0020	0.023 (0.027)	0.010 (0.013)	0.016 (0.019)	0.019 (0.026)	0.122 (0.106)	0.122 (0.127)	0.101 (0.100)	0.151 (0.127)		0.032
0.0025	0.038 (0.046)	0.013 (0.017)	0.026 (0.035)	0.030 (0.037)						0.090
0.0030	0.062 (0.079)	0.021 (0.023)	0.046 (0.043)	0.041 (0.060)	0.221 (0.191)	0.213 (0.209)	0.180 (0.166)	0.256 (0.180)		0.256
0.0035	0.084 (0.116)	0.029 (0.034)	0.073 (0.066)	0.063 (0.076)						
0.0040	0.152 (0.150)	0.048	0.100 (0.082)	0.087 (0.100)	0.273 (0.223)	0.282 (0.257)	0.283 (0.196)	0.337 (0.198)		
0.0050					0.351 (0.232)	0.349 (0.283)	0.359 (0.267)	0.457 (0.258)		

<sup>(a)</sup>The number in parentheses were tests conducted under a negative mean strain ( $\epsilon_m$ ). The mean strains used were 0.004 (A514), 0.005 (A36), and 0.003 (5083-0). All values of k are negative.

<sup>(b)</sup>Actual strain amplitudes ( $\epsilon_a$ ) were 0.0011, 0.0020, 0.0026, 0.0030.

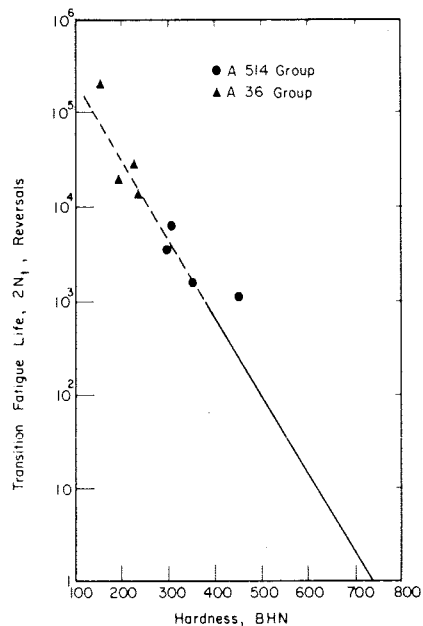


Fig. 16—Transition fatigue life ( $2N_{1/2}$ ) as a function of hardness<sup>33</sup>

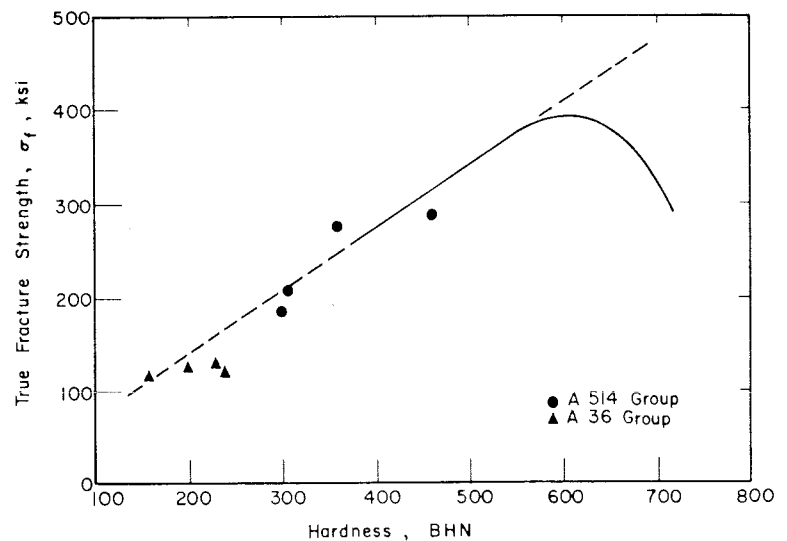


Fig. 17—True fracture strength ( $\sigma_f$ ) as a function of hardness<sup>33</sup>

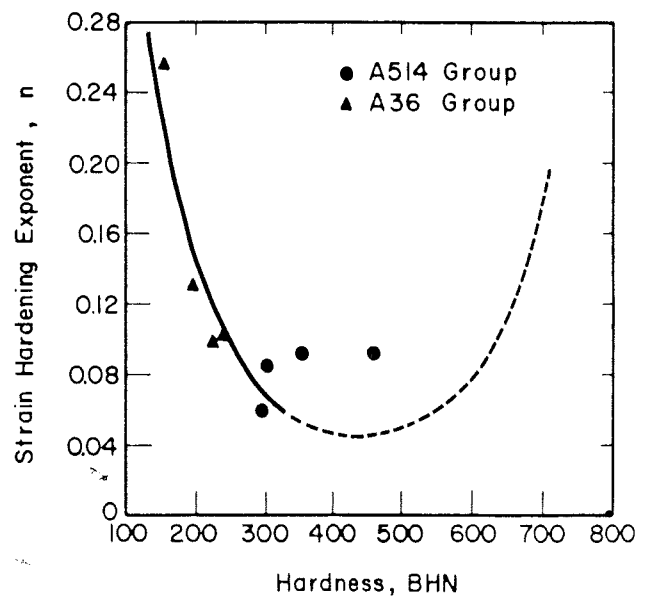
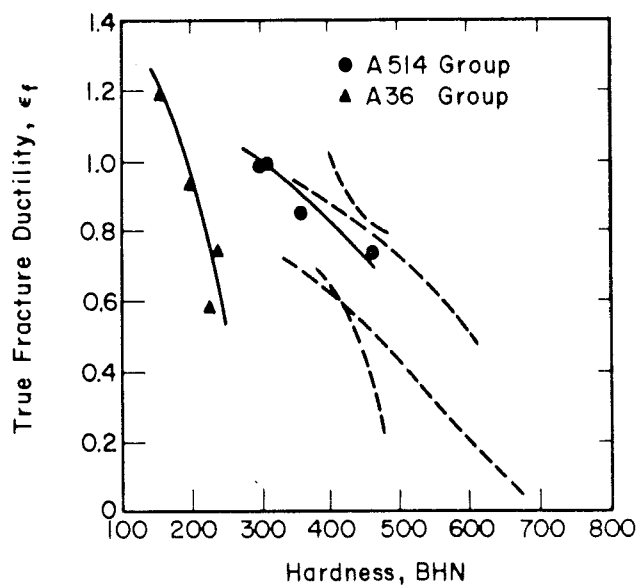


Fig. 18—Monotonic strain hardening exponent ( $n$ ) and true fracture ductility ( $\epsilon_f$ ) as a function of hardness<sup>33</sup>

Ship Systems Command, Grant N00024-73-C-5344. Mechanical testing and metallography was performed in the laboratories of the Departments of Metallurgy and Mining, Civil Engineering, and Theoretical and Applied Mechanics at the University of Illinois, Urbana, Illinois.

References

1. Lawrence, F. V., Jr., and Radziminski, J. B., "Fatigue Crack Initiation and Propagation in High-Yield-Strength Steel Weld Metal," *Welding Journal*, 49 (10), Oct. 1970, Research Suppl., pp. 445-s to 452-s.
2. Gurney, T. A., *Fatigue of Welded Structures*, Cambridge University Press, Cambridge, U. K., 1968.
3. Pollard, B., and Cover, R. J., "Fatigue of Steel Weldments," *Welding Journal*, 51 (11), Nov. 1972, Research Suppl., pp. 544-s to 554-s.
4. Burk, J. D., and Lawrence, F. V., Jr., "The Effect of Lack-of-Penetration and Lack-of-Fusion on the Fatigue Properties of 5083-0 Aluminum Alloy Welds," *Welding Research Council Bulletin No. 234*, January 1978.

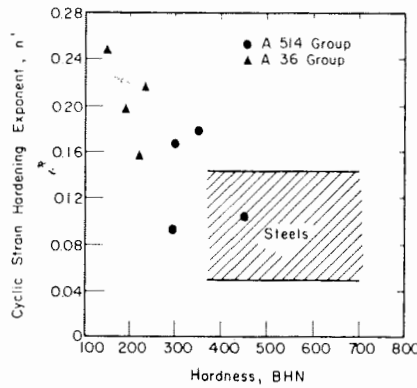


Fig. 19—Cyclic strain hardening exponent ( $n'$ ) as a function of hardness<sup>33</sup>

5. Lancaster, J. F., *The Metallurgy of Welding, Brazing and Soldering*, American Elsevier, New York, 1965.
6. Maddox, S. J., "Fatigue Crack Propagation in Weld Metal and HAZ," *Metal Construction and British Welding Journal*, Vol. 2, No. 7, 1970, pp. 285-289.

7. Maddox, S. J., "Some Further Fatigue Crack Propagation Results Relevant to Welded Joints in Steel," *British Welding Institute Members' Report E/37/70*, 1970.
8. Maddox, S. J., "Fatigue Crack Propagation Data -Obtained from Parent Plate, Weld Metal and HAZ in Structural Steels," *British Welding Institute Members' Report E/48/72*, 1972.
9. Maddox, S. J., "Some Further Fatigue Crack Propagation Results Relevant to Welded Joints in Steel," *British Welding Research International*, Vol. 3, No. 1, 1973, pp. 72-99.
10. Dowse, K. R., and Richards, C. E., "Fatigue Crack Propagation Through Weld Heat Affected Zone," *Metallurgical Transactions*, Vol. 2, No. 2, 1971, pp. 599-603.
11. Bucci, R. J., Clark, W. G., Jr., and Paris, P. C., "Fatigue Crack Propagation Growth Rates under a Wide Variation of  $\Delta K$  for an ASTM A517 Grade F (T-1) Steel," *Stress Analysis and Growth of Cracks, Proceeding of the 1971 National Symposium on Fracture Mechanics, Part I*, ASTM STP 513, American Society for Testing and Materials, 1972, pp. 177-195.
12. Parry, M., Nordberg, H., and Hertz-

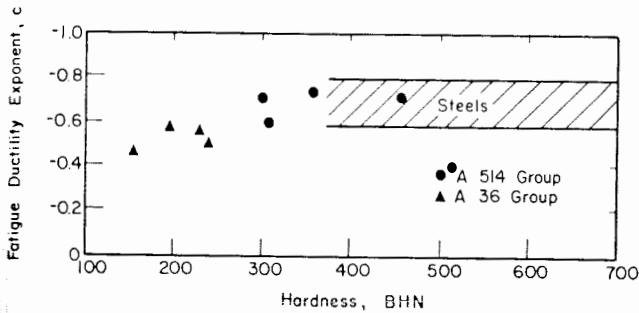


Fig. 20—Fatigue ductility ( $c$ ) and strength ( $b$ ) exponents as a function of hardness<sup>33</sup>

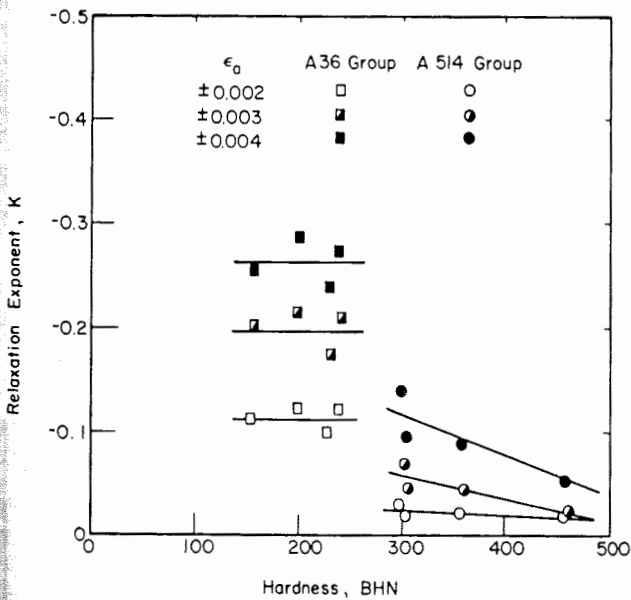
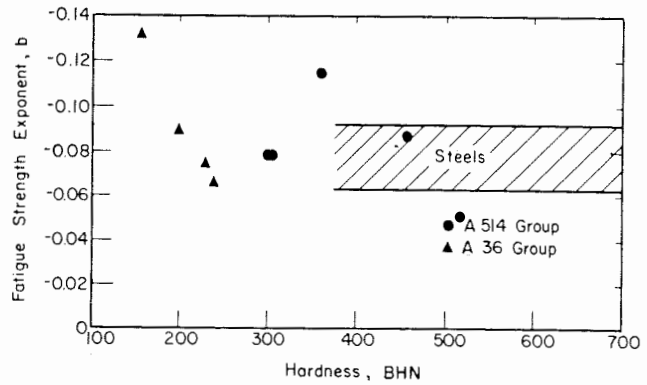
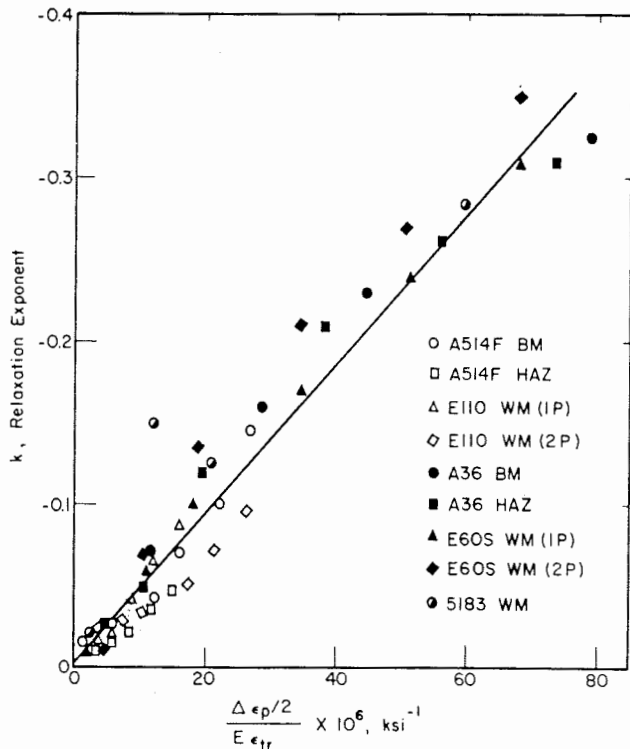


Fig. 21—Relaxation exponent ( $k$ ) as a function of hardness

Fig. 22—Relaxation exponent ( $k$ ) as a function of plastic strain amplitude ( $\Delta \epsilon_p/2$ ) and elastic modulus ( $E$ ) and transition strain ( $\epsilon_{tr}$ )



berg, R. W., "Fatigue Crack Propagation in A514 Base Plate and Welded Joints," *Welding Journal*, 51 (10), Oct. 1972, Research Suppl., pp. 485-s to 490-s.

13. Flanigan, A. E., and Kaufman, M., "Microcracks and the Low-Temperature Cooling Rate Embrittlement of Welds," *Welding Journal*, 30 (12), Dec. 1951, Research Suppl., pp. 613-s to 622-s.

14. Ohta, S., and Satoh, S., "Fatigue Properties in Notched Steel Plates and the Effects of Welding on Them (Report 1)," *Journal of the Japan Welding Society*, Vol. 44, No. 9, 1975, pp. 65-72.

15. Watanabe, M., Nagai, K., Otsuka, A., and Nagata, Y., "A Study of Fatigue Strength in Weld Metal and HAZ of Mild Steel Weld," *Journal of the Japan Welding Society*, Vol. 36, No. 4, 1967, pp. 55-63.

16. Kenyon, N., Morrison, W. B. and Quarrell, A. G., "Fatigue Strength of Welded Joints in Structural Steels," *British Welding Journal*, Vol. 13, No. 3, 1966, pp. 123-137.

17. Muraki, J., Ishiguro, T. and Yokota, H., "Fatigue Characteristics of Weld Heat Affected Zone in High Tensile Strength Steels, Treated with a Synthetic Apparatus for Weld Thermal Cycles (Report 1)," *Journal of the Japan Welding Society*, Vol. 36, No. 3, 1967, pp. 27-35.

18. Muraki, J., Ishiguro, T. and Yokota, H., "Fatigue Characteristics of Weld Heat Affected Zone in High Tensile Strength Steels, Treated with a Synthetic Apparatus for Weld Thermal Cycles (Report 2)," *Journal of the Japan Welding Society*, Vol. 37, No. 9, 1968, pp. 64-68.

19. Nippes, E. F., "The Weld Heat-

Affected Zone," *Welding Journal*, 38 (1), Jan. 1959, Research Suppl., pp. 1-s to 18-s.

20. Lowes, J. M., Richardson, K. D., and Haddrill, D. M., "Thermal Simulator Employing Induction Heating," *Metal Construction and British Welding Journal*, Vol. 4, No. 10, 1972, pp. 373-375.

21. Nippes, E. F., and Savage, W. F., "Development of Specimen Simulating Weld Heat-Affected Zones," *Welding Journal*, 28 (11), Nov. 1949, Research Suppl., pp. 534-s to 546-s.

22. Clifton, T. E., and George, M. I., "Design and Construction of a Weld Heat-Affected Zone Simulator," *Metal Construction and British Welding Journal*, Vol. 1, No. 9, 1969, pp. 427-431.

23. Dolby, R. E., and Widgery, D. J., "The Simulation of HAZ Microstructures," *Welding Research International*, Vol. 1, No. 4, 1971.

24. Grover, H. K., and Jolly, G., "Fracture Characteristics of Simulated HAZs in a Low-Alloy Constructional Steel," *Metal Construction and British Welding Journal*, Vol. 5, No. 7, 1973, pp. 250-252.

25. Suzuki, H., and Tamuar, H., "Synthetic Heat Affected Zone Ductility Test," *Transactions of National Research Institute for Metals (Japan)*, Vol. 1, No. 2, 1959, pp. 119-125.

26. Mattos, R. J., "Estimation of the Fatigue Crack Initiation Life in Welds Using Low Cycle Fatigue Concepts," Ph.D. Thesis, University of Illinois at Urbana-Champaign, Urbana, Illinois, 1975.

27. Burk, J. D., "Predicted Effects of Residual Stresses on Butt Weld Fatigue

Life," Ph.D. Thesis, University of Illinois at Urbana-Champaign, Urbana, Illinois, 1978.

28. Morrow, J., "Cyclic Plastic Strain Energy and Fatigue of Metals," *Internal Friction, Damping and Cyclic Plasticity*, ASTM STP 378, American Society for Testing and Materials, 1965, pp. 45-87.

29. Morrow, J., "Fatigue Properties of Metals," Section 3.2 of *Fatigue Design Handbook*, Grahm, J., Editor, Society of Automotive Engineers, New York, 1968.

30. Jhansale, H. R., and Topper, T. H., "Engineering Analysis of the Inelastic Stress Response of a Structural Metal under Variable Cyclic Strains," *Cyclic Stress-Strain Behavior—Analysis, Experimentation, and Failure Prediction*, ASTM STP 519, American Society for Testing and Materials, 1973, pp. 246-270.

31. Feltner, C. E., and Mitchell, M. R., "Basic Research on the Cyclic Deformation and Fracture Behavior of Materials," *Manual on Low Cycle Fatigue Testing*, ASTM STP 465, American Society for Testing and Materials, 1969, pp. 27-66.

32. Slot, T., Stentz, R. H., and Berling, J. T., "Controlled-Strain Testing Procedures," *Manual on Low Cycle Fatigue Testing*, ASTM STP 465, American Society for Testing and Materials, 1969, pp. 100-128.

33. Landgraf, R. W., "Cyclic Deformation and Fatigue Behavior of Hardened Steels," Ph.D. Thesis, University of Illinois at Urbana-Champaign, Urbana, Illinois, 1969.

34. Morrow, J., Halford, G. R., and Millan, J. F., "Optimum Hardness for Maximum Fatigue Strength of Steel," *Proceedings of the First International Conference on Fracture*, Vol. 3, 1965, pp. 1611-1635.

## To Update Your Book "Weldability of Steels" You Can Now Order Revised WRC Bulletin 191 March 1978

### Suggested Arc-Welding Procedures for Steels Meeting Standard Specifications

by C. W. Ott and D. J. Snyder

The authors of WRC BULLETIN 191 have completely revised the 40-page table "Steel Compositions with Suggested Practices Generally Required for Sound Welding" and the list of steels specified by ASTM, AISI, SAE and API.

This revised Bulletin incorporates all of the changes and additions that have been made in the list of the steels specified by the above organizations through June 1977.

Consequently, the second edition of the book, "Weldability of Steels" by R. D. Stout and W. D. Doty, which was published by WRC in 1971, and WRC BULLETIN 191, published in January 1974, can be brought up-to-date by purchasing a copy of REVISED BULLETIN 191 MARCH 1978.

Publication of this revised Bulletin was sponsored by the Weldability (Metallurgical) Committee of the Welding Research Council.

The price of Revised Bulletin 191 is \$9.00 per copy. Orders should be sent with payment to the Welding Research Council, 345 E. 47th St., New York, NY 10017.